Comprehensive Glare Hazard Analysis of Ethylene Tetrafluoroethylene (ETFE) Based Frontsheet for Flexible Photovoltaic Applications

Sreejith, K. P.; Venkatesh, Vijay ; Padmakumar, Govind; Smets, Arno H.M.

DOI
10.1109/JPHOTOV.2024.3463961

Publication date
2024

Document Version
Final published version

Published in
IEEE Journal of Photovoltaics

Comprehensive Glare Hazard Analysis of Ethylene Tetrafluoroethylene (ETFE) Based Frontsheet for Flexible Photovoltaic Applications

K. P. Sreejith, Vijay Venkatesh, Govind Padmakumar, and Arno H. M. Smets

***Abstract*—Photovoltaic (PV) panel installations in buildings and transportation hubs pose additional safety challenges as the glare from the panels can impose adverse impacts like flash blindness in human eyes. This study substantiates that polymer encapsulated thin film modules offer significantly low glare levels that are essential for building integrated and transport hub installations. In this work, the glare hazard potential associated with matt ethylene tetrafluoroethylene (ETFE)-based polymer sheet used as the frontsheet for the production of flexible thin amorphous silicon (a-Si) PV modules is studied and compared with standard PV glass used in crystalline silicon (c-Si) PV panels. The specular reflectance extracted from the measured total and diffuse reflectance for an angle of incidence (AOI) of 8° and the angular intensity distribution (AID) of specular reflectance measured for AOI ranging from 10° to 80° are utilized for glare assessment of the frontsheets. The mean value of specular reflectance extracted from the measured total and diffused reflectance is as low as $<0.5\%$ for the polymer frontsheet and is $>4\%$ for glass. The AID measurements suggest that the reflection from the polymer frontsheet is highly diffusive in nature in contrast to glass and the measured specular reflectance is always close to a magnitude lower than that from glass for all AOI. With the increase in AOI, the specular AID reflectance increases exponentially for glass to become as high as 40%, which is almost 20 times less than that from the polymer frontsheet for an AOI of 80°. Further, the c-Si test structure with glass and thin a-Si PV module with matt ETFE-based polymer as frontsheet showed similar specular reflectance trends as that of glass and the polymer frontsheet, respectively.**

***Index Terms*—Amorphous silicon solar panels, flexible power foils, glare hazard analysis, reliability of photovoltaic devices, specular reflectance.**

I. Introduction

THE transition from conventional fossil fuel sources of energy to low-carbon sources of energy is inevitable to bring down global warming to pre-industrial levels. As of 2023, photovoltaic (PV) technology holds the largest share of installed capacity in the renewable energy sector with a share of 14% [1]. An impressive growth of up to 22% is projected by 2027, to become the largest installed power capacity surpassing coal [1]. This translates to 2.7 TW of PV installation by 2027, and such a tremendous growth demands PV installations such as building integrated (BIPV), vehicle integrated (VIPV) in urban and metropolitan areas, transportation hubs such as railway stations and airports, and their surroundings.

Conventional crystalline silicon PV technology uses rigid low iron content tempered glass for encapsulating the solar cells. The typical weight of the glass encapsulated modules lies in the range of 12–16 kg-m^{-2} and glass accounts for nearly 60%–70% of the total module weight [2], [3]. This limits the use of glass encapsulated panels in portable PV, and BIPV applications. Replacement of the glass with a lightweight flexible polymer sheet can substantially reduce the weight of PV modules. However, such polymer sheets are required to meet stringent properties such as high transparency, a similar index of refraction as that of glass, resilience to harsh environmental conditions, and protect the cells from contaminants, moisture, water ingress, and dust particles. Polycarbonate, polyethylene terephthalate (PET), and ethylene tetrafluoroethylene (ETFE) are some of the commonly explored polymer frontsheets for the production of light-weight PV panels [4], [5], [6]. However, in reference to glass, both polycarbonate and PET sheets have a higher index of refraction values that leads to higher reflection losses [7]. ETFE sheets are commonly used in plastic industries due to their desired properties like flexibility, durability, and high electrical and chemical resistance [8], [9], [10]. In addition, chemical stability against extreme weather conditions and UV radiation, high transmission, and low index of refraction as compared to other polymer sheets make the ETFE polymer sheet a good choice as frontsheet material [11], [12], [13], [14]. In this context, a recent study demonstrated that ETFE sheets are not only resistant to the IEC 61215 standard protocol-based acceleration tests such as damp heat, UV exposure, and hail tests, but also have a hydrophobic surface with higher water contact angle that can lead to lower soiling losses [15]. These studies suggest the potential of ETFE sheets as a frontsheet for the production of flexible PV modules.

The glare induced from the reflective surfaces can cause ocular impact and hence, reflections from PV panels can be a serious concern, especially for BIPV, VIPV, and transportation

Received 11 May 2024; revised 22 July 2024 and 6 September 2024; accepted 16 September 2024. Date of publication 15 October 2024; date of current version 21 October 2024. This work was supported by the bilateral "HyET Solar—TU Delft" research contract. *(Corresponding author: K. P. Sreejith.)*

The authors are with the Faculty of Electrical Engineering, Mathematics, and Computer Science, Delft University of Technology, 2628 CD Delft, The Netherlands (e-mail: S.KoorthedathPullayikody@tudelft.nl; A.H.M.Smets@tudelft.nl).

Color versions of one or more figures in this article are available at https://doi.org/10.1109/JPHOTOV.2024.3463961.

Digital Object Identifier 10.1109/JPHOTOV.2024.3463961

hub installations. As per the literature, retinal irradiance in the range of 0.1–kW-m^{-2} induces flash blindness or discomfort to human eyes [16], [17], [18], [19]. However, there are still no well defined international standards available to evaluate glare hazard from PV panels for various applications, and the available regulations are mainly for installations in airports and their premises. Previous studies reported that PV installations in the vicinity of airports induce glare onto the flight path, consequently jeopardizing pilots' visibility during takeoff and landing phases [16], [20], [21], [22]. Airport regulatory authorities of different countries such as the United States, United Kingdom, Germany, and Switzerland have set up their own regulations for addressing the glare hazard from PV installations [23], [24], [25], [26]. Solar Glare Hazard Analysis Tool (SGHAT) developed by Sandia National Laboratories in the United States, helicopter flyover approach using a heliostat, and the usage of software packages in computational fluid dynamics are some of the reported methods used for glare assessment of PV installations near the airport premises [27], [28], [29], [30]. However, most of the above approaches are either based on computational methods that use predefined reflectance profiles [31], [32] or are only for certain PV configurations for a fixed module tilt [21], [33]. In contrast, a recent study utilized gonioreflectometry measurement-based bidirectional reflectance distribution function (BRDF) to asses the glare from PV modules encapsulated with six different glass for a varied angle of incidence (AOI) of up to 75° [19]. The study demonstrated that glare from glass encapsulated modules can be a serious concern, especially for higher AOI, and glare hazards from smooth, textured, and antireflective (AR) coated glass surfaces are significantly different [19], [34]. The results also indicate that the glare from PV panels will be different for different PV materials and installation conditions like module tilt. Hence, it is extremely important to investigate the glare hazard associated with the frontsheet used in PV modules, especially for BIPV, VIPV, and transport hub-related installations.

This work compares the glare associated with two frontsheets; glass and an ETFE-based polymer sheet, which are used for the encapsulation of crystalline silicon (c-Si) wafer-based and thin amorphous silicon (a-Si)-based solar panels, respectively. Glare hazard was evaluated based on the specular reflectance obtained from the integrating sphere spectrophotometer measurements for an AOI of 8° and from the angular intensity (AID) measurements for a varied AOI of 10° to 80°. The study reveals that in reference to glass, the reflection from the matt ETFE-based polymer sheet is diffusive in nature even for shallow AOI. Hence, ETFE-based polymer encapsulated PV modules do not induce severe glare as in the case of glass encapsulated modules and are more suitable for areas of PV installations, where glare can be a serious concern.

II. Experimental Details

A. Sample Details and Fabrication of Test Structure

A flexible polymer top encapsulant (PTE) sheet and PV-grade glass used for the encapsulation of flexible a-Si power foils and c-Si solar panels, respectively, are characterized in this study for their glare. The PTE sheet consists of two matt ETFE sheets of ~ 40 μm thick sandwiched using silicone glue. This configuration of the PTE sheet is used to enhance mechanical strength and is a proprietary item of HyET Solar B.V., a manufacturer of thin flexible a-Si PV modules. The top-down SEM images of the matt ETFE surface are shown in Fig. 1. Several micron-sized craters are seen all over the ETFE surface, which can enhance the light scattering compared to flat surface. The selected reference glass is a PV grade, low iron content, front side flat, and rear side textured type, which is designed for a balanced soiling and cell-to-module loss. The measured total reflectance and transmittance curves of the glass and the PTE sheet are shown in Fig. 2. The transmittance of both glass and the PTE sheet is as high as 90%–95% for the wavelength range of 400 to 700 nm. Glass samples showed marginally higher transmittance for lower wavelength ranges and the PTE sheet exhibited better response for higher wavelength ranges. The reflectance curves of both the frontsheets are discussed in detail in the upcoming sections. Further, the glare hazard from the glass encapsulated c-Si and ETFE-based polymer encapsulated thin film a-Si panels are studied by fabricating a 5 cm $\times$ 5 cm sized representative c-Si PV module test structure and by cutting a slice of 5 cm $\times$ 5 cm from a flexible single junction a-Si module, respectively. The schematic representation of the cross-sectional view of the glass encapsulated c-Si test structure and a thin a-Si PV module are shown in Fig. 3. The c-Si test structure consists of a random pyramid alkaline textured mono-crystalline wafer with 75–80 nm thick plasma enhanced chemical vapor deposited

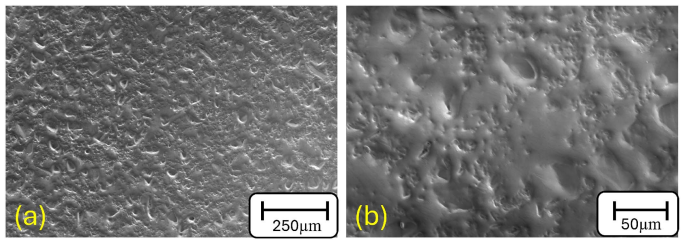

Fig. 1. Top-down SEM images of matt ETFE surface at at two different magnifications; (a) low and (b) high resolution..

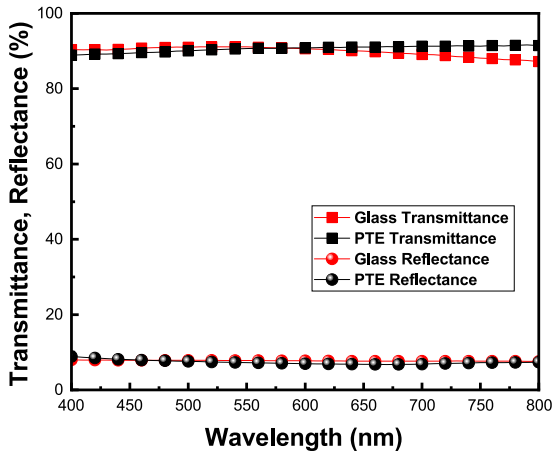

Fig. 2. Wavelength dependant reflectance and transmittance plots of glass and PTE sheet.

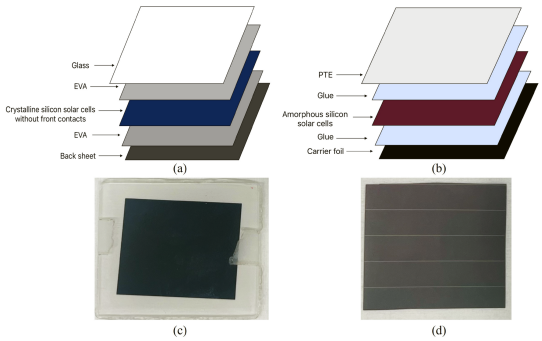

Fig. 3. Cross-sectional schematics of PV modules: (a) Glass-encapsulated c-Si test structure and (b) ETFE-encapsulated a-Si thin film flexible module. Visuals: (c) c-Si test structure and (d) a-Si thin film flexible module.

silicon nitride (SiN_X:H) AR coating at the front and screen printed aluminium (Al) contact at the rear. Further, the wafer was encapsulated with glass (at the front side) and a white back sheet (at the rear side) using an ethylene vinyl acetate (EVA) sheet as the cross-linking layer to complete the fabrication of glass encapsulated c-Si test structure. The exact process parameters and optical properties of the encapsulant materials used are available in [35], [36], and [37]. In contrast, as indicated in Fig. 3(b), a-Si power foil panels are encapsulated with flexible polymer sheets on both sides; PTE at the front and a carrier foil at the rear. The a-Si solar cell structure includes a p-i-n single junction structure with fluorine-doped tin oxide as the front contact, zinc oxide (ZnO) as a buffer layer between the front contact and the p layer, and a combination of ZnO and Al as back contact.

B. Characterization

The total transmittance, total reflectance, and diffuse reflectance are measured using an integrating sphere spectrophotometer; Lambda 1050 from Perkin Elmer. The schematic representation of the integrating sphere spectrophotometer is shown in Fig. 4(a) . The sample holder position is fixed and the light beam is always incident on the sample surface at an angle of 8°. The detector is in the shape of a sphere to integrate the light scattered in all directions (except the opening area through which the light is incident on the sample). During the diffused reflectance measurements, a removable slot present in the detector is removed to exclude the specular component of reflection. Further, the AID measurement was employed for analyzing the reflection from sample surfaces for varied AOI. Schematic representation of the absolute reflectance transmittance accessory (ARTA) tool from OMT Solutions BV used for AID measurements is shown in Fig. 4(b). Here, the sample stage can move from the vertical position (θ_s=0°) to the horizontal position (θ_s=90°) corresponding an AOI of 0° to 90°, respectively. In addition, for a fixed AOI, the detector moves along the 180° covering the entire plane of reflection (i.e., θ_d changes from $-90° + \theta_s$ to $90° + \theta_s$) from the sample surface. However, the detector possesses a miniintegrating sphere arrangement that records the reflectance only in the direction of the plane of incidence. Also, as indicated in Fig. 4(b), the detector movement in the direction ranging from $-10°$ to 10° is restricted as it corresponds to the slit through which the light beam is incident on to the sample surface.

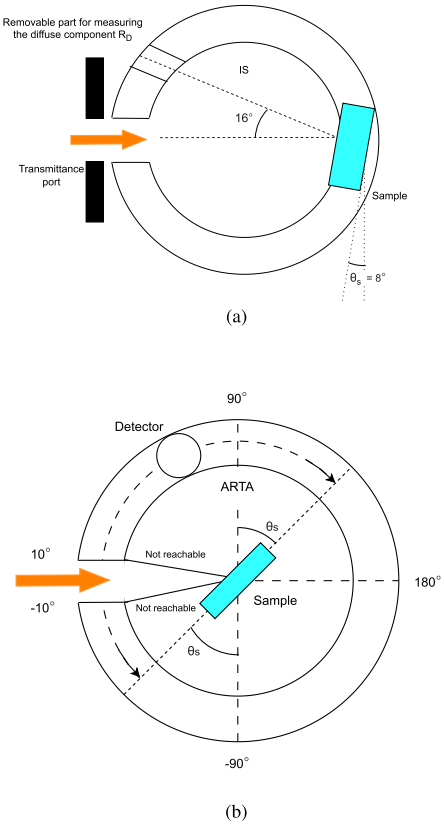

Fig. 4. Schematic representation of the (a) integrating-sphere spectrophotometer and (b) AID measurement systems. (a) Integrating-sphere spectrophotometer measurement setup (b) Angular intensity distribution measurement setup.

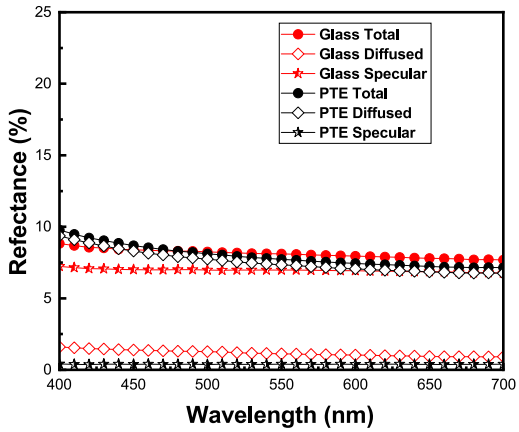

Fig. 5. Measured total, diffused, and extracted specular reflectance curves of top encapsulation layers; glass and ETFE-based PTE sheet.

III. Results and Discussion

A. Integrating Sphere Spectrophotometer Measurements

The measured total and diffused reflectance curves of the glass and PTE sheet are shown in Fig. 5. Further, the specular reflectance curve is extracted by subtracting the diffused reflectance from the total reflectance. Both glass and the PTE

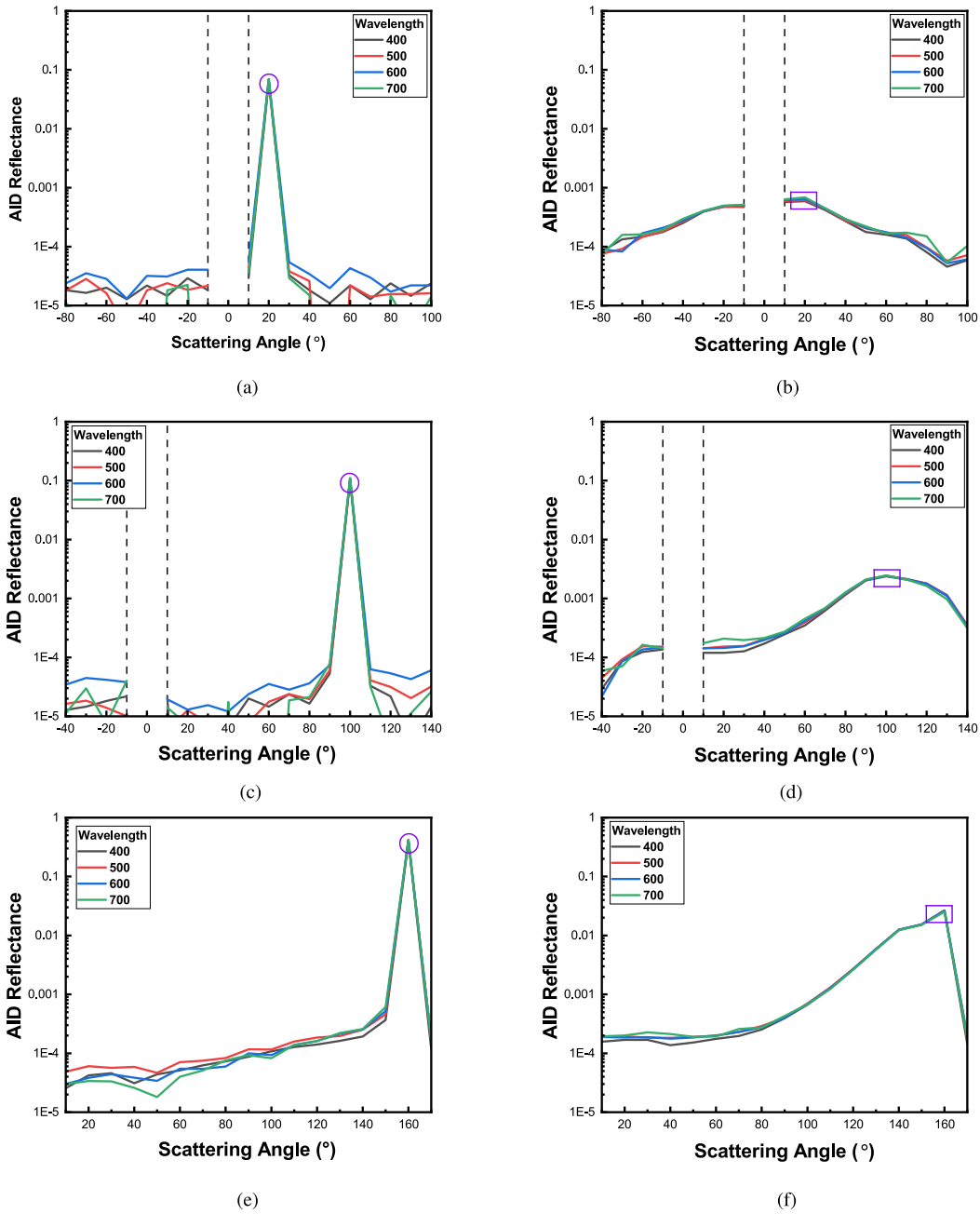

Fig. 6. AID reflectance plots of glass and PTE sheet samples for an AOI of (a) and (b) 10°, (c) and (d) 50°, and (e) and (f) 80°. (a) Glass with AOI of 10° (b) PTE with AOI of 10° (c) Glass with AOI of 50° (d) PTE with AOI of 50° (e) Glass with AOI of 80° (f) PTE with AOI of 80°.

sheet exhibited comparable total reflection with a mean value of 8.11% and 7.93%, respectively over the wavelength range of 400 to 700 nm. However, the measured diffused reflectance values are significantly different for the glass and PTE samples, with the former having a mean value of only 1.16% and the latter with 7.55%. This suggests that the reflection from the PTE surface is highly diffusive in nature in contrast to glass and the specular component of reflectance responsible for glare is as low as below 0.5% for an AOI of 8°. However, for building integrated and transport hub installations, it is essential to assess the glare for the entire AOI range to account for the varied module installation tilt and the movement of the sun during the day.

B. ARTA Measurements

The AID reflectance of glass and PTE sheet for an AOI of 10°, 50°, and 80° are shown in Fig. 6. Both glass and PTE samples follow a near-normal scattering distribution for all three AOI. The peak maximum intensity (marked with a circle and rectangular box, respectively, for glass and PTE, in Fig. 6) of the

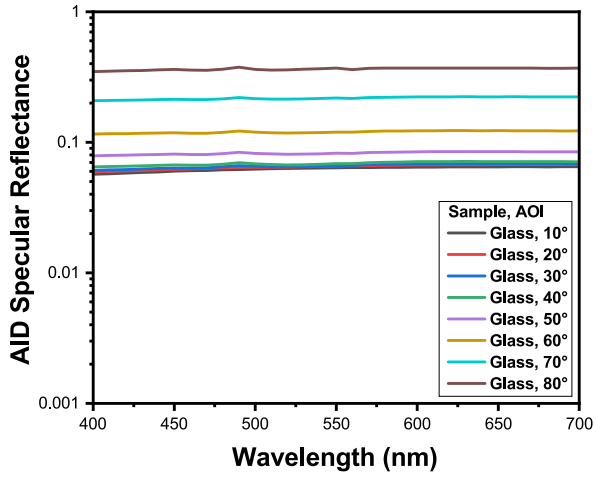

(a) Glass

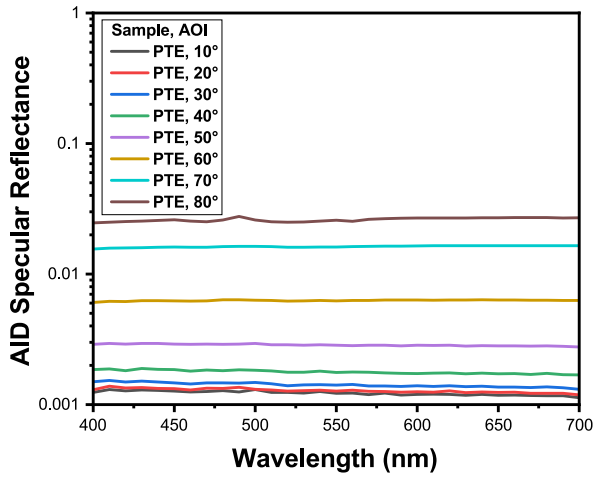

(b) PTE

Fig. 7. Variation in specular AID reflectance for (a) glass and (b) PTE sheet for different AOI from 10° to 80°. (a) Glass (b) PTE.

normal distribution is obtained at an angle twice that of AOI and hence, it represents the magnitude of AID specular reflectance. For both the samples, the specular AID reflectance increases with increases in AOI, indicating that the glare hazard from the frontsheets becomes severe for shallow AOI. For all three AOI, glass displays a compact distribution with a large fraction of the total reflectance as specular itself. In reference to peak intensity, the reflectance measured at other scattering angles is significantly lower for glass. In contrast, the PTE sheet showed a broader distribution with a lower peak intensity as compared to glass for all three AOI. This indicates that the reflection from the PTE sheet is more diffusive than that from glass even for shallow AOI as high as 80°. The AID reflectance distribution of the PTE sheet gets more compact and the peak intensity representing the AID specular reflectance increases for higher AOI. Even though the diffusive nature of reflection from the PTE surface reduces for higher AOI, the overall AID reflectance and magnitude of specular reflectance from the PTE sheet are still substantially broader and significantly lower compared to glass.

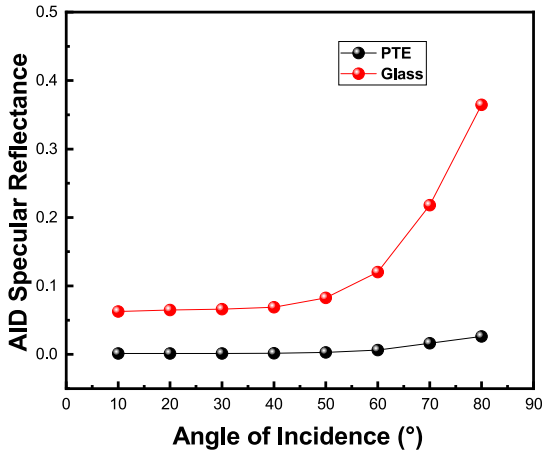

Fig. 8. Variation of mean specular AID reflectance for glass and PTE for different AOI.

Further, the wavelength-dependant AID specular reflectance curves (the AID reflectance measured at an angle twice that of AOI) of glass and PTE sheet for AOI ranging from 10° to 80° are plotted in Fig. 7. The specular reflectance trends, especially for AOI of 10° are in agreement with the specular reflectance curves shown in Fig. 5, wherein both the cases, the specular reflection from glass is nearly an order magnitude higher than from the PTE sheet. Interestingly, the AID specular reflectance from the PTE sheet at an AOI of 80° is still lower than that from the glass for an AOI of 10° . The specular AID reflectance from the PTE sheet is always below 0.03 for the entire wavelength range from 400 to 700 nm for all AOI ranging from 10° to 80°. In contrast, for glass, the specular AID reflectance is always higher than 0.06 and exceeds 0.1 for AOI beyond 50°.

The mean value of AID specular reflectance for both glass and PTE sheet are plotted for varied AOI from 10° to 80° in Fig. 8. The mean value is obtained by averaging the wavelength-dependent specular AID in Fig. 7. From Fig. 8, it can be seen that the glass exhibits an exponential increase in specular reflectance for higher AOI. For an AOI of 80°, the specular AID from glass was as high as 0.4. The reflection trends for glass are in agreement with available literature [38], [39] and such a high specular reflection can lead to glare levels above the threshold for ocular discomfort [17], [18], [19]. In contrast, the increase in specular reflectance for higher AOI is marginal for the PTE sheet. These specular AID reflectance values indicate that for all AOI, the glare level from PTE samples will remain below 50 W-m^{-2} even for a high-intensity incident irradiance of 1000 W-m^{-2}. These results confirm that the PTE sheets do not induce glare levels that can result in ocular discomfort as in the case of glass and hence, are widely used for building integrated applications.

C. Glare Hazard From Glass and PTE Encapsulated Samples

Further, the glare hazard from the glass encapsulated test structure and PTE encapsulated a-Si flexible module are analyzed and compared with glass and the PTE sheet. The total, diffused, and extracted specular reflectance of glass encapsulated test structure and a-Si flexible module is shown in Fig. 9.

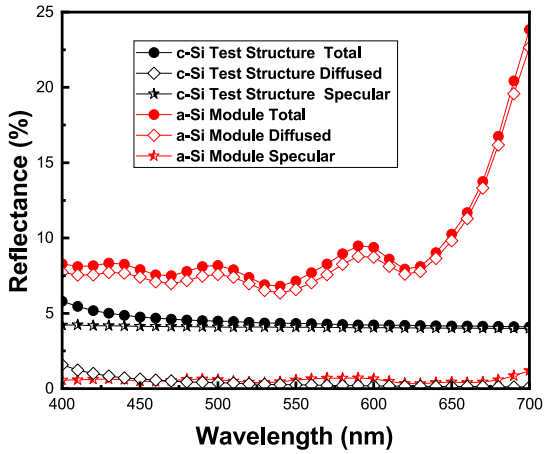

Fig. 9. Measured total, diffused, and extracted specular reflectance curves of glass encapsulated c-Si test structure and polymer encapsulated a-Si thin-film module.

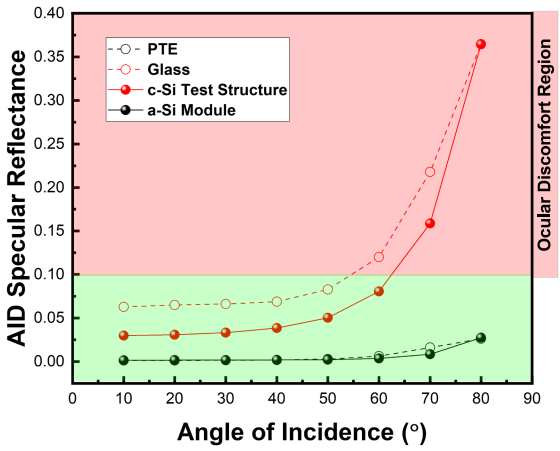

Fig. 10. Variation of mean specular AID reflectance of glass encapsulated module test structure and PTE encapsulated a-Si module for different AOI. Curves with dotted lines represent the specular AID reflectance for reference glass and PTE sheet.

The total reflection from the a-Si panel is higher than the c-Si module. The mean value of total reflectance corresponding to glass encapsulated c-Si test structure and polymer encapsulated a-Si modules are 5.19% and 9.31%, respectively. The mean value of measured diffused reflectance was only 1.04% and as high as 8.74%, respectively, for glass encapsulated c-Si test structure and thin a-Si flexible module. This suggests that the reflection from the glass encapsulated module and PS encapsulated a-Si module, respectively, are specular and diffusive, in accordance with the reflectance trends seen in the case of glass and the PTE sheet. Further, it can also be concluded that the frontsheet determines the nature of reflection from the PV panels. Similar to glass and PTE samples, the specular component of reflection from a thin a-Si module is nearly an order magnitude lower than from glass encapsulated c-Si test structure for an AOI of 8°.

The mean specular AID reflectance from glass encapsulated and polymer encapsulated samples are shown in Fig. 10. The dashed line represents the specular AID trends for glass and the PTE sheet, discussed in Fig. 8. The variation in the magnitude of AID specular reflectance between the frontsheet materials and encapsulated structures can be attributed to the complex interplay of light coupling at various interfaces. However, it can be clearly seen that glass encapsulated c-Si test structure and polymer encapsulated a-Si module, respectively, follow the trends of glass and the PTE sheet. This suggests that the top layer used in encapsulation determines the glare hazard from PV panels for all AOI. As discussed earlier, a retinal irradiance of > 100 W-m^{-2} (i.e., 10% of one sun illumination intensity) induces discomfort to human eyes and hence, AID specular reflectance of 0.1 is considered here as the threshold for glare from PV panels. For AOI beyond 60°, the glare levels from glass and glass encapsulated modules (region marked with a red rectangular box in Fig. 10) are severe enough to cause ocular discomfort. The results obtained for reference glass are in agreement with the BRDF measurements shown in a previous study [19]. Importantly, the specular reflection from PTE and polymer encapsulated samples are comfortably below the threshold required to cause discomfort to human eyes. Hence, thin film PV panels with PTE as the frontsheet are a favorable choice for BIPV and transport hub installation considering their low glare hazard along with their flexibility and lightweight.

IV. Conclusion

This work demonstrates that the matt ETFE-based frontsheet instead of glass significantly lowers the glare hazard from PV panels below the threshold levels for ocular discomfort. The specular component of reflection obtained from the integrating sphere spectrophotometer and AID measurements were utilized for assessing the glare from the glass and the PTE sheet. For a fixed AOI of 8°, the mean value of specular reflection obtained from integrating sphere measurements was less than 0.5% for the PTE sheet and was close to 7% for glass. The AID measurements further confirm that the reflection from PTE is diffusive in nature for all AOI ranging from 10° to 80° and the specular AID reflectance is consistently an order magnitude lower for PTE than glass. Moreover, both glass encapsulated c-Si test structure and PTE a-Si panels follow similar specular reflectance trends as that of glass and the PTE sheet, respectively, suggesting that the top layer of the encapsulated module determines the scattering nature of reflection from the PV panels. Further, in contrast to glass encapsulated PV module structures, PTE encapsulated a-Si panels produce glare comfortably below the threshold levels mentioned in the available literature. Hence, thin-film PV panels with a matt ETFE-based polymer sheet as the frontsheet fulfil both flexibility and low glare, which are essential for transportation hubs and BIPV installations.

Acknowledgment

The authors would like to thank all the students and staff members of the Thin Film PV cluster of Photovoltaic Materials and Devices (PVMD) group at the Delft University of Technology for all their support, and the R&D team of HyET Solar B. V. for providing the polymer frontsheets and flexible a-Si power foils. The authors would also like to thank Dr. Subhendu Guha for his guidance, discussions, and critical feedback on the work.

REFERENCES

[1] International Energy Agency, "Executive summary renewables," 2022. Accessed: Mar. 31, 2024. [Online]. Available: https://www.iea.org/reports/renewables-2022/executive-summary

[2] A. C. Martins, V. Chapuis, A. Virtuani, and C. Ballif, "Robust glass-free lightweight photovoltaic modules with improved resistance to mechanical loads and impact," *IEEE J. Photovolt.*, vol. 9, no. 1, pp. 245–251, Jan. 2019.

[3] F. Ferroni and R. J. Hopkirk, "Energy return on energy invested (ERoEI) for photovoltaic solar systems in regions of moderate insolation," *Energy policy*, vol. 94, pp. 336–344, 2016.

[4] A. Budiman et al., "Enabling lightweight polycarbonate-polycarbonate (PC-PC) photovoltaics module technology–enhancing integration of silicon solar cells into aesthetic design for greener building and urban structures," *Sol. Energy*, vol. 235, pp. 129–139, 2022.

[5] K. Mik, P. Zawadzki, J. Tarłowski, and S. Bykuć, "Assessment of prototype lightweight photovoltaic modules after over 1-year field test in polish conditions," *Renewable Energy*, vol. 198, pp. 1008–1020, 2022.

[6] T. Tachibana, K. Shirasawa, and K. Tanahashi, "Development of lightweight and flexible crystalline silicon solar cell modules with PET film cover for high reliability in high temperature and humidity conditions," *Sol. Energy Mater. Sol. Cells*, vol. 262, 2023, Art. no. 112541.

[7] X. Zhang, J. Qiu, X. Li, J. Zhao, and L. Liu, "Complex refractive indices measurements of polymers in visible and near-infrared bands," *Appl. Opt.*, vol. 59, no. 8, pp. 2337–2344, 2020.

[8] J. Hu et al., "Structural behavior of the PV–ETFE cushion roof," *Thin-Walled Structures*, vol. 101, pp. 169–180, 2016.

[9] C. Lamnatou, A. Moreno, D. Chemisana, F. Reitsma, and F. Clariá, "Ethylene tetrafluoroethylene (ETFE) material: Critical issues and applications with emphasis on buildings," *Renewable Sustain. Energy Rev.*, vol. 82, pp. 2186–2201, 2018.

[10] J. Hu, W. Chen, B. Zhao, and D. Yang, "Buildings with ETFE foils: A review on material properties, architectural performance and structural behavior," *Construction Building Mater.*, vol. 131, pp. 411–422, 2017.

[11] P. Good et al., "Spectral reflectance, transmittance, and angular scattering of materials for solar concentrators," *Sol. Energy Mater. Sol. Cells*, vol. 144, pp. 509–522, 2016.

[12] R. French, J. Rodríguez-Parada, M. Yang, R. Derryberry, and N. Pfeiffenberger, "Optical properties of polymeric materials for concentrator photovoltaic systems," *Sol. Energy Mater. Sol. Cells*, vol. 95, no. 8, pp. 2077–2086, 2011.

[13] R. French et al., "Optical properties of materials for concentrator photovoltaic systems," in *2009 34th IEEE Photovoltaic Specialists Conf. (PVSC)*, IEEE, 2009, pp. 000394–000399.

[14] T. M. Hammam, B. Alhalaili, M. Abd El-sadek, and A. A. Abuelwafa, "Effect of protective layer on the performance of monocrystalline silicon cell for indoor light harvesting," *Sensors*, vol. 23, no. 18, p. 7995, 2023.

[15] F. Lisco et al., "ETFE and its role in the fabrication of lightweight c-si solar modules," *IEEE J. Photovolt.*, vol. 13, no. 3, pp. 349–354, May 2023.

[16] C. K. Ho and C. M. Ghanbari, "Hazard analyses of glint and glare from concentrating solar power plants," Sandia National Lab.(SNL-NM), Albuquerque, NM, USA, Tech. Rep. SAND2009-4131C, 2009.

[17] G. Bargary, Y. Jia, and J. L. Barbur, "Mechanisms for discomfort glare in central vision," *Invest. Ophthalmol. Vis. Sci.*, vol. 56, no. 1, pp. 464–471, 2015.

[18] R. Schregle, C. Renken, and S. Wittkopf, "Spatio-temporal visualisation of reflections from building integrated photovoltaics," *Buildings*, vol. 8, no. 8, p. 101, 2018.

[19] M. Babin, S. Thorsteinsson, M. L. Jakobsen, and S. V. Spataru, "Glare potential evaluation of structured PV glass based on gonioreflectometry," *IEEE J. Photovolt.*, vol. 12, no. 6, pp. 1314–1318, Nov. 2022.

[20] S. Sreenath, K. Sudhakar, and A. F. Yusop, "Solar photovoltaics in airport: Risk assessment and mitigation strategies," *Environ. Impact Assessment Rev.*, vol. 84, Sep. 2020, Art. no. 106418, doi: 10.1016/j.eiar.2020.106418.

[21] S. Sreenath, K. Sudhakar, and F. Yusop, "Solar PV in the airport environment: A review of glare assessment approaches & metrics," *Sol. Energy*, vol. 216, pp. 439–451, Mar. 2021.

[22] S. Sreenath, K. Sudhakar, and A. Yusop, "Solar PV in the airport environment: A review of glare assessment approaches & metrics," *Sol. Energy*, vol. 216, pp. 439–451, 2021.

[23] Federal Aviation Administration, "FAA policy: Review of solar energy system projects on federally-obligated airports," May 2021. Accessed: Mar. 31, 2024. [Online]. Available: https://www.federalregister.gov/documents/2021/05/11/2021-09862/federal-aviation-administration-policy-review-of-solar-energy-system-projects-on-federally-obligated

[24] Civil Aviaiton Authority United Kingdom, "Interim CAA guidance - solar photovoltaic systems," 2010. Accessed: Mar. 31, 2024.

[25] Ministry of the Environment, Health and Consumer Protection, "Guideline on the measurement and assessment of light immissions," 2014, as amended by order of the MLUK on 17 Sep. 2021. Official Journal 21, No 40, p. 779. Original version: Official Journal 14, No 21, p. 691.

[26] D. Stickelberger and C. Moll, "Guide to solar systems according to art. 18a of the spatial planning act," *Swissolar (Swiss Assoc. Sol. Energy)*, 2016.

[27] C. Ho, "Relieving a glaring problem," *Solar Today*, American Solar Energy Society, vol. 27, pp. 28–31, 2013.

[28] C. K. Ho, "Observations and assessments of glare from heliostats and trough collectors: Helicopter flyover and drive-by sightings," Sandia National Lab. (SNL-NM), Albuquerque, NM, USA, No. SAND2011-5667C, 2011.

[29] C. K. Ho, C. M. Ghanbari, and R. B. Diver, "Methodology to assess potential glint and glare hazards from concentrating solar power plants: Analytical models and experimental validation," *ASME. J. Sol. Energy Eng.*, vol. 133, no. 3, 2011.

[30] T. Rose and A. Wollert, "The dark side of photovoltaic–3D simulation of glare assessing risk and discomfort," *Environ. Impact Assessment Rev.*, vol. 52, pp. 24–30, 2015.

[31] C. K. Ho, C. A. Sims, J. Yellowhair, and E. Bush, "Solar glare hazard analysis tool (SGHAT) technical reference manual," Sandia National Laboratories, Albuquerque, USA, 2015.

[32] Forge solar help. Accessed: Mar. 31, 2024. [Online]. Available: https://www.forgesolar.com/help/

[33] F. J. Moralejo-Vázquez, N. Martín-Chivelet, L. Olivieri, and E. Caamaño-Martín, "Luminous and solar characterization of PV modules for building integration," *Energy Buildings*, vol. 103, pp. 326–337, 2015.

[34] J. Moereke et al., "Light reflection analysis of PV modules: Comparison to building facades and assessing the possibility of glare," in *Proc. 8th World Conf. Photovoltaic Energy Convers., Milan*, 2022, pp. 1050–1056.

[35] P. K. Basu, K. Sreejith, T. S. Yadav, A. Kottanthariyil, and A. K. Sharma, "Novel low-cost alkaline texturing process for diamond-wire-sawn industrial monocrystalline silicon wafers," *Sol. Energy Mater. Sol. Cells*, vol. 185, pp. 406–414, 2018.

[36] T. J. Nath, K. Sreejith, and A. Kottantharayil, "Assessment of optical properties of metal assisted chemically etched black silicon surface morphology in multi-crystalline cells and modules by ray-tracer simulations," in *2020 5th IEEE Int. Conf. Emerg. Electron. (ICEE)*, IEEE, 2020, pp. 1–4.

[37] K. Sreejith, T. J. Nath, and A. Kottantharayil, "Comprehensive cell to module optical loss analysis of metal assisted chemically etched inverted pyramid textured multi-crystalline silicon solar cells and modules by ray-tracing method," *Sol. Energy*, vol. 244, pp. 315–321, 2022.

[38] D. Rüdisser, R. McLeod, W. Wagner, and C. Hopfe, "Numerical derivation and validation of the angular, hemispherical and normal emissivity and reflectivity of common window glass," *Building Environ.*, vol. 207, 2022, Art. no. 108536.

[39] R. Danks, J. Good, and R. Sinclair, "Avoiding the dreaded death ray: Controlling facade reflections through purposeful design," in *Proc. Façade Tectonics World Congress*, Los Angeles, CA, USA, 2016.